3.5 Shock joining

The reader of Sections 3.3 and 3.4 has seen a variety of shock waves, or 'shocks', composed of abrupt or discontinuous changes in the depth or width of the flow within which the semigeostrophic and/or hydrostatic approximations break down. Examples include the advancing Kelvin wave bores in the Rossby adjustment problem (Figures 3.3.6 and 3.3.7), the Kelvin wave hydraulic jump and upstream bore (Figure 3.4.11) and the transverse hydraulic jumps and bores (Figure 3.4.8, 3.4.9, and 3.4.12). We now take a closer look at these features by exploring the relationship between the flow immediately upstream and downstream of the abrupt transition. The problem of connecting these end states is known as *shock joining*. As a simple model, we will consider a hypothetical discontinuity in fluid depth occurring along a contour C (Figure 3.5.1). For the time being, it will be assumed that the fluid depth remains non-zero over C. Away from C the fluid motion is governed by the shallow water equations. It will be helpful to use a Cartesian coordinate system (n,s), placed such that n is aligned normal to and s parallel to C at the point P. The coordinate system remains fixed but C moves at speed $c^{(n)}$ in the n-direction.

If the system is one of reduced gravity, where the moving surface is an interface separating fluids of different densities, then the discontinuity may be associated with mixing of the two fluids. Closure of the shock joining problem then requires further assumptions or approximations. These difficulties have yet to be resolved in the current literature and will be avoided in the present discussion by limiting discussion to flows with a free surface.

A reader of Section 1.6 has seen two methods for obtaining the matching conditions across a shock. Both treat the shock as a discontinuity in d, v, etc. that exists in the presence of gradually varying topography. The approach that is most general, if not most popular, is to formulate the primitive conservation statements on mass and momentum over a control volume containing the discontinuity. Since the volume contains no sources of mass or momentum the conserved quantities are the volume flux and the flow 'force' (momentum flux plus pressure force). We will discuss the same procedure as applied to the shock of Figure 3.5.1.

The second approach is to integrate the shallow water equations over a small interval that contains the discontinuity. This method is generally less trustworthy because the equations themselves may not be valid within the region of rapid transition. Use of different forms of the shallow water equations yield different results. For example, integration of the common form (see 2.1.1 and 2.1.2) of the momentum equations, yields the incorrect result that energy is conserved across the shock. The correct procedure is to write the equations so that they take the form of conservation laws for the quantites (in this case the volume flux and flow force) that are known to be preserved. The reasoning here is somewhat circular: one must know in advance which properties are to be conserved, and this knowledge derives from the fundamental reasoning behind the primitive control volume formulation! In fact, the desired 'flux'

form of the momentum equations is that which follows directly from the control volume derivations.[1] Nevertheless, the approach is widespread and flexible: once the correct governing equations are known, they can be applied to a variety of shocks with differing structure and geometry. We will illustrate both methods, beginning with the primitive control volume approach. The following discussion is based largely on Pratt (1983b) and Schär and Smith (1993). Some of the basic ideas can be traced back to Crocco, as described by Batchelor, 1967 Section 3.5).

a. Shock joining by control volumn analysis.

Consider the force and mass budgets within a small box containing the shock, as shown in Figure 3.5.2a,b. The sides have length 2ε width $2l$ and the box extends from the bottom to the free surface. The box is fixed in space and is aligned so that its sides are parallel or perpendicular to n. It is assumed the velocity through edges of the box conform to the shallow-water approximation and, in particular, is depth-independent, except possible where the edges are intersected by the discontinuity.

The rate of change of n-momentum within the box must be balanced by the net flux of n-momentum into the box and the sum of the forces in the n-direction acting on the sides. One type of momentum flux is the normal flux $d\left(u^{(n)}\right)^2$ across sides 1 and 2. Since $u^{(n)}$ is expected to be discontinuous across the shock, the difference in these normal fluxes remains finite as ε is decreased but decreases in proportion to l as the l is decreased. Similarly, the depth-integrated pressure, nondimensionally $\frac{1}{2}d^2$, over side 1 is different from that over side 2, even as ε as decreased. All other forces and fluxes go to zero more rapidly as the box is shrunk. The tangential flux of normal momentum ($d u^{(s)} u^{(n)}$) over sides 3 and 4 of the box are continuous in the s-direction and their difference decreases in proportion to εl as the box is shrunk. The Coriolis acceleration leads to a 'force' proportional to the integral of $du^{(s)}$ over the area of the box and is therefore proportional to εl. The same can be said for any contribution from bottom drag or topographic slope. Thus, as ε and l are decreased, the momentum budget reduces to

$$\frac{d}{dt}\iiint_V v\,dr \approx 2l\left[\tfrac{1}{2}(d_2^2 - d_1^2) + (d_2 v_2^2 - d_1 v_1^2)\right]$$

where V is the volume of the box. The left-hand integral reduces to $2lc^{(n)}(d_2 u_2^{(n)} - d_1 u_1^{(n)})$ as ε and l are reduced[2] and the matching conditions is thus

$$c^{(n)}\left\langle u^{(n)} d\right\rangle - \left\langle u^{(n)2} d + \tfrac{1}{2}d^2\right\rangle = 0\,, \qquad (3.5.1)$$

[1] For example, the Section 1.10 control volume derivation (see Figure 1.10.3) leads directly to a flux form (Equation 1.10.4) of the momentum equations.

[2] A similar calculation was performed in connection with equation 1.6.8.

where $\langle(\ )\rangle = \lim_{\varepsilon\to 0}[(\ )_2 - (\ )_1]$.

A similar treatment of the mass balance easily leads to

$$c^{(n)}\langle d\rangle - \langle u^{(n)} d\rangle = 0\,. \tag{3.5.2}$$

So far, the matching conditions are identical to take those found in a single dimension *y*, provided that *y* is identified with normal direction *n*. However the tangential momentum balance (Figure 3.5.2b) is more subtle. Here the leading contribution comes from the difference in the normal flux of tangential momentum, proportional to the difference in $du^{(s)}u^{(n)}$ between sides 1 and 2. The flux $d\left(u^{(s)}\right)^2$ of tangential momentum and the pressure vary continuously between sides 3 and 4, and their difference leads to a negligible contribution as the box is shrunk. The same can be said for the contributions due to the Coriolis acceleration acting on the net normal velocity, the bottom drag, and topographic pressure. The result is that the change in net tangential momentum within the box, $c^{(n)}\langle u^{(s)} d\rangle$, is balanced by the difference in the normal flux of tangential momentum $\langle u^{(s)}u^{(n)}d\rangle$:

$$c^{(n)}\langle u^{(s)} d\rangle - \langle u^{(s)}u^{(n)}d\rangle = 0\,, \tag{3.5.3}$$

Together with (3.5.2), this result implies that the tangential velocity $u^{(s)}$ is conserved across the discontinuity:

$$\langle u^{(s)}\rangle = 0\,. \tag{3.5.4}$$

Note that (3.5.1) and (3.5.2) are identical to the conditions (1.6.4) and (1.6.5) governing one-dimensional shocks provided that the one-dimensional fluid velocity and shock speed are interpreted as $v^{(n)}$ and $c^{(n)}$. As a result, many of the properties of one-dimensional discontinuities apply locally to the two-dimensional, rotating discontinuities. For example, a stationary discontinuity requires that the local normal velocity of the upstream state be 'supercritical' $u_u^{(n)} > (d_u)^{1/2}$ (*cf.* Equation 1.6.7).

b. Shock joining using the flux form of the shallow water equations.

The correct matching conditions have been established as conservation laws for the flow for the normal fluxes of volume and tangential momentum, and for the normal component of flow force. It follows that the same conditions are derivable though

integration of the differential form of these conservation laws, also the form that follows directly from the control volume analysis for a continuous flow. An interested reader might want to review the discussion in Section 1.10, in which a control volume derivation leads directly to a flux form (Equation 1.10.4) of the momentum equations. The two-dimensional form of these equations is given by (2.1.17), which can be written in the present coordinate system as

$$\frac{\partial(u^{(n)}d)}{\partial t}+\frac{\partial}{\partial n}(u^{(n)2}d+\tfrac{1}{2}d^2)+\frac{\partial(u^{(n)}u^{(s)}d)}{\partial s}=-d\frac{\partial h}{\partial n}+du^{(s)}+dF^{(n)} \qquad (3.5.5a)$$

and

$$\frac{\partial(u^{(s)}d)}{\partial t}+\frac{\partial(u^{(n)}u^{(s)}d)}{\partial n}+\frac{\partial}{\partial s}(u^{(s)2}d+\tfrac{1}{2}d^2)=-d\frac{\partial h}{\partial x}-u^{(n)}d+dF^{(s)} \qquad (3.5.5b)$$

To these we may add the continuity equation (2.1.7), expressed as

$$\frac{\partial d}{\partial t}+\frac{\partial}{\partial n}\left(u^{(n)}d\right)+\frac{\partial}{\partial s}\left(u^{(s)}d\right)=0\,, \qquad (3.5.6)$$

and already in the desired form.

Integration of (3.5.6) over a small interval $[-\varepsilon \le n \le \varepsilon]$ about the shock at this point results in

$$\int_{-\varepsilon}^{\varepsilon}\frac{\partial d}{\partial t}dn+\left[u^{(n)}d\right]_{n=\varepsilon}-\left[u^{(n)}d\right]_{n=-\varepsilon}+\int_{-\varepsilon}^{\varepsilon}d\frac{\partial u^{(s)}}{\partial s}dn=0\,.$$

The first integral can be written as

$$\frac{\partial}{\partial t}\int_{-\varepsilon}^{\varepsilon}(d)dy=\frac{\partial}{\partial t}\int_{-\varepsilon}^{n_c(t)}(d)dy+\frac{\partial}{\partial t}\int_{n_c(t)}^{\varepsilon}(d)dy$$

where $n_c(t)$ is the position of the discontinuity on the n-axis. If ε is reduced to zero, the right-hand side approaches $-c^{(n)}\langle d\rangle$, where $c^{(n)}=\partial n_c/\partial t$ and $\langle d\rangle$ is the change in d across the discontinuity, as defined earlier. Since the shock is parallel to the n-axis, the s-derivative in (3.5.1) is bounded along this integration path and thelast integral in the same equation is made arbitrarily small by letting ε approach zero. The general constraint imposed by mass conservation can thus reduces to (3.5.2).

We leave it as an exercise for the reader to show that a similar integration, applied to (3.5.5a,b), yields the correct conditions (3.5.1) and (3.5.3).

c. Consequences of the shock joining conditions.

If $u^{(s)} \neq 0$ then the change in $u^{(n)}$ required by (3.5.2) implies that the velocity vector $\boldsymbol{u}=(u^{(n)},u^{(s)})$ must point in different directions on either side of a shock. Along a horizontal wall with free slip, the velocity vector is clearly aligned parallel to the wall regardless of whether a shock is present. These two facts can be reconciled only if C is aligned perpendicular to the wall at a point of contact, otherwise a flow into the boundary would be induced. In our slowly varying channel, where the walls are aligned in the y-direction, or nearly so, a shock must be aligned in the x-direction near the walls. One might now ask whether we can invoke the semigeostrophic approximation $v>>u$ right up to the shock, which would force the shock to lie in the x-direction all across the channel. If so, one could start with a specified, geostrophically balanced $v(y)$ and $d(y)$ immediately upstream of a hydraulic jump and use (3.5.1) and (3.5.2) to compute $v(y)$ and $d(y)$ immediately downstream. However, since the shock-joining conditions do not depend on the Coriolis parameter, there is no guarantee that the downstream v will be geostrophically balanced; in general it will not be so. In summary, the semigeostrophic equations are not generally valid right up the shock, nor must the shock remain aligned with x away from the channel walls. Since rotational effects generally require a finite distance (the deformation radius) over which to act, we anticipate the existence of a transitional region around C within which the semigeostrophic far field flow adjusts to the (possibly) non-geostrophic flow at C.

This expectation is confirmed by the cross-stream momentum balance within the leading edge of the upstream-propagating 'Kelvin' bore of Figure 3.4.11. The momentum balance (Figure 3.5.3) is nearly geostrophic at t=20, but becomes less so with time. The primary source of contamination is the development of strong, cross-channel accelerations within the steepening regions of the bore, an effect evidenced by the growth of the term $\partial u / \partial t$. By t=80 the bore has steepened to the point where the depth changes occur over a fraction of a deformation radius L_d $(= (gD_\infty)^{1/2} / f)$. However, the ageostrophic region extends approximately 1/2 deformation radius upstream and downstream of the zone of rapid depth change.

Following the above remarks, one might expect a discontinuity in depth to occur within an ageostrophic region R that extends a distance $O(L_d)$ downstream and possibly upstream (Figure 3.5.4). The 'shock' might now be considered as whole region R with its imbedded discontinuity. R is joined upstream and downstream to semigeostrophic flows. It will be assumed that the flow in R is steady, but the same analysis can be carried out in the moving frame of the shock that translates at a steady speed c. The central problem of shock joining is to predict the downstream semigeostrophic end state given the upstream end state (and, in the case of a moving shock, the speed c). If the potential vorticity distribution $q(\psi)$ is preserved as the flow passes through R, then the shock joining problem is straightforward. For the $q(\psi)$ given by the known upstream condition, the downstream end state is found by solving the second order equation (2.2.2). The resulting profile of downstream depth, and the corresponding geostrophic velocity would then be known within two integration constants. These constants could be determined by two additional constraints, one being conservation of the total volume flux. A second

constraint is provided by the conservation of the total (width integrated) flow force:[3] : $\int_{-w/2}^{w/2}\left[v^2 d + \tfrac{1}{2}d^2\right]dx$. In summary, the conservation of volume flux, $q(\psi)$, and total flow force through *R* should be sufficient to close the problem.

Success of this procedure depends on potential vorticity conservation across the discontinuity, and we now ask whether this is consistent with (3.5.1, 3.5.2 and 3.5.4). Begin with the property that the Bernoulli function and potential vorticity are related by $q=dB/d\psi$, where ψ represents the streamfunction of the steady flow seen in the frame of reference moving with the steadily propagating shock. Since mass is conserved across the discontinuity, we have $\langle d\psi \rangle = 0$ and therefore

$$\langle q \rangle = \left\langle \frac{dB}{d\psi} \right\rangle = \frac{\langle dB \rangle}{d\psi}. \qquad (3.5.7)$$

In addition, the jump in the value of *B* can be written in terms of the jump in depth using the previously derived relation (1.6.6) for energy dissipation, nondimensionally expressed as

$$\langle B \rangle = -\frac{\langle d \rangle^3}{4 d_d d_u}. \qquad (3.5.8)$$

Here d_u and d_d are the depths immediately upstream and downstream of the discontinuity at the point of interest. Thus

$$\langle q \rangle = -\frac{d}{d\psi}\frac{\langle d \rangle^3}{4 d_d d_u} = \frac{1}{[u^{(n)} d]_{u \text{ or } d}}\frac{d}{ds}\frac{\langle d \rangle^3}{4 d_d d_u} \qquad (3.5.9)$$

where the final derivative is taken along the shock, as shown in Figure 3.5.4. The normal velocity $u^{(n)}$ is that seen in the moving frame. An observer facing the shock from upstream sees a positive normal velocity entering the shock, with ψ decreasing, and *s* increasing, from right to left. The dimensional version of (3.5.9) is obtained by multiplying its right-hand side by *g* and regarding all other variables as dimensional.

d. Geostrophic shocks.

Nof (1986) presents a special class of shocks that can be described analytically and for which the potential vorticity change can be calculated. The procedure is to look

[3] The width-integrated flow force is conserved provided the horizontal component of bottom or side-wall pressure within *R* is not important. In a gradually varying channel, the length scale *L* of topographic and width variations is large compared to the length L_d of *R* and therefore the bottom and side-wall pressure alter the momentum flux through *R* by only an $O(L_d/L)$ amount.]

for a solution in which the channel flow is parallel (v=0), and therefore geostrophic, right up to the discontinuity. The latter is assumed to be aligned in the x-direction so that C consists of a straight line perpendicular to the channel axis (Figure 3.5.5). Under the restrictions that both end states are parallel, and therefore geostrophically balanced, and that (3.5.1, 3.5.2, and 3.5.4) are satisfied at each x, a special class of upstream states can be found that permit stationary shocks with the assumed properties. As noted above, the upstream state must be 'locally supercritical' $v>d^{1/2}$ at each y. The results are classified in terms of two parameters: a Froude number $F_w = v_u\big|_{x=w/2} / d_u^{1/2}\big|_{x=w/2}$ and Rossby number $v_u(w/2)/w$, both based on right-wall values of the upstream flow. A set of examples of upstream and downstream depth profiles with fixed Rossby number are shown in Figure 3.5.6. Starting with the value F_w=1, where there is no discontinuity, the jump $\langle d \rangle$ in depth across the shock tends to increase as F_w increases. In each case, $\langle d \rangle$ tends to increase from left-to-right and, according to (3.5.9), this is consistent with an increase in potential vorticity for the fluid passing through the discontinuity. The computed increases are shown in Figure 3.5.7 for a particular value of $v_u(w/2)/w$. Note that these changes can be O(1). Potential vorticity changes are also present in the various shocks discussed on Section 3.4.

e. Vorticity generation in shocks.

The non-conservation of potential vorticity across a shock can give rise to interesting downstream effects including jets and vortex streets. Consider a nonrotating jump in a channel with a rounded cross-section (Figure 3.5.8). This feature was modeled by Siddall et al. (2004) as part of a simulation of an ancient flood thought to have occurred in the Black Sea. The flow immediately upstream of the jump is parallel and uniform (u=0, v=constant) and therefore q_u=0. The jump consists of an abrupt, nearly uniform increase in the free surface elevation and thus the depth difference $(d_d(s) - d_s(s))$ is therefore constant. The differentiated term on the right-hand side of (5.3.9) is therefore controlled by the denominator, which decreases to the left and right of the channel center. The differentiated term therefore increases away from the channel center and it follows that q_d>0 to the left and q_d<0 to the right. With the neglect of f, q_d is proportional to the vorticity of the fluid downstream of the jump, the distribution of which is consistent with a jet-like velocity profile, as produced by a numerical simulation (Figure 3.5.9).

Vorticity production within a jump can be explored further by considering a helpful form of the vorticity equation (see Exercise 1 or Section 2.1)

$$\frac{\partial \zeta_a}{\partial t} + \nabla \cdot \left[\mathbf{u}\zeta_a + \mathbf{J}_n \right] = 0 \,, \qquad (3.5.10)$$

(see Exercise 1 of Section 2.1). In this dimensionless form, $\zeta_a = 1 + \zeta$ is the absolute vorticity and $\mathbf{J}_n = \mathbf{k} \times \mathbf{F}$, where $\mathbf{F}$ contains the dissipation and horizontal body force. For the flows under consideration, the later is generally zero and we will think of $\mathbf{J}_n$ as arising only from dissipation. The vorticity flux vector $\mathbf{u} \cdot \zeta_a + \mathbf{J}_n$ is then composed of an advective part $\mathbf{u} \cdot \zeta_a$ plus a dissipative part.

Taking the cross-product of $\mathbf{k}$ with the dimensionless, steady version of (2.1.15) yields

$$\mathbf{k} \times \nabla B = \mathbf{u}\zeta_a + \mathbf{J}_n , \qquad (3.5.11)$$

which shows that the Bernoulli function acts as a streamfunction for the vorticity flux (Schär and Smith, 1993)[4]. Since $\mathbf{u}$ is parallel to streamlines, the derivative of B along them gives a contribution that is entirely due to dissipation. If the dissipation is zero, the vorticity flux is entirely due to advection and is proportional to the derivative of B in the cross-streamline direction. In the treatment of shocks we generally consider the dissipation to be negligible outside the region of rapid or discontinuous change.

A nice application of these ideas is to atmospheric wakes in the lee of islands and mountains (e.g., Smith et al. 1997). For the islands in question, the effects of Earth's rotation are generally weak. The reduced airflow in the wake reduces the sea surface roughness, resulting in 'shadows' in the sea surface glint patterns (e.g. Figure 3.5.10). In an idealized view of the wake, the winds approaching the island are uniform and are confined to a shallow surface layer that obeys the reduced-gravity version of our shallow water equations. When the approach flow is subcritical and the island is not so high that it protrudes through the upper interface, the fluid spilling over the top can become supercritical and form a hydraulic jump (Figure 3.5.11). Regions of cyclonic and anticyclonic shear are also observed downstream of the jump and these are indicated in the figure. In some cases the vorticity is collected in a vortex street, a train of staggered eddies of alternating sign (Figure 3.5.12). If the approach flow is uniform and inviscid, the downstream vorticity must be generated by the jump.

The discontinuity in depth is largest at the center (y=0) of the jump and (3.5.8) suggests that the loss in Bernoulli function should also be largest there. The flow immediately downstream of the jump should therefore have a minimum in B at x=0 and B should increase as one moves along the jump in either direction (to the right of left, facing downstream). It is also assumed that B is conserved along streamlines ($\mathbf{J}_n$=0) in the downstream region, changes having already taken place where the streamline passed through the jump. The y-component of (3.5.11) for the flow immediately downstream of the jump is $\partial B / \partial x = v\zeta_a$, where v>0 and $\partial B / \partial x$ is >0 for x>0 and is <0 for x<0. The vorticity ζ_a, which is dominated by the relative vorticity ζ in these applications is therefore positive on the right-hand side of the wake (facing downstream) and negative on the left side. Since the approach flow has zero vorticity, the positive and negative

[4] The inviscid form of (3.5.11) is related to a more general result obtained by Crocco (1937).

vorticity must have been generated within the jump and could account for the vorticity in the alternating eddies. The time-dependent aspect of the alternating eddies requires an additional instability mechanism that is not explored here.

A complementary result can be found by applying (3.5.11) to the interior of the jump itself. To do so, it must be assumed that the rapid change in depth occurs over a small but finite distance and that (3.5.11) continues to hold within. Consider the component of this equation tangential to the jump. If one temporarily considers x to be the tangential direction, then this component is given by $-\partial B/\partial y = u\zeta_a + J^{(x)}$. Integration of this relation across the small interval ($-\varepsilon \le y \le \varepsilon$, say) of rapid depth change yields

$$\int_{-\varepsilon}^{\varepsilon} (u\zeta + J_n^{(x)})dy = -(B|_{x=\varepsilon} - B|_{x=-\varepsilon}) > 0 .$$

The left-hand term can be interpreted as a vorticity flux tangent to the jump (Figure 3.5.11), positive in the left-to-right direction (facing downstream). Its magnitude is zero at the extremities of the jump and therefore its divergence is positive over the left portion and negative over the right portion. A positive divergence is consistent with the generation of negative vorticity in the jump, whereas a convergent flux indicates a generation of positive vorticity. Both tendencies are in agreement with the vorticity carried away from the jump by the fluid.

Exercises

1. Deduce the inviscid form of (3.5.11) directly from the relation $q=dB/d\psi$?

2. For the nonrotating hydraulic jump shown in Figure 3.5.11 in which the depth is maximum at the centerline and the upstream velocity is uniform across the channel, show that the change in potential vorticity produces a downstream vorticity distribution (cyclonic on the left and anticyclonic on the right side of the channel) consistent with a jet.

Figure Captions

Figure 3.5.1 Definition sketch showing discontinuity in depth $\boldsymbol{C}$ that moves normal to itself at speed $c^{(n)}$ at the point P.

Figure 3.5.2 Control volumes (viewed from above) with (a) fluxes of momentum normal to the jump and (b) fluxes of momentum tangential to the jump.

Figure 3.5.3 The frames on the left show the longitudinal sections of the surface elevation for the flow of Figure 3.4.11 at various times. The three sections in each frame are taken at the channel centerline and walls: $x=0$ and $x=\pm w/2$. The frames on the right

show the terms in the *y*-momentum balance at the channel centerline over the interval indicated by vertical bars in the corresponding figure to the right.

Figure 3.5.4 Idealized view of the ageostrophic region *R* and the imbedded depth discontinuity.

Figure 3.5.5 The shock hypothesized by Nof (1986). The depth discontinuity is perpendicular to the channel walls and the parallel, geostrophically balanced, upstream and downstream flows join directly to the discontinuity. (There is no adjustment region.)

Figure 3.5.6 Upstream and downstream depth profiles for a shock of the type shown in Figure 3.5.5. The governing upstream parameters are a Froude number $F_w = v_u(w/2)/d_u^{1/2}(w/2)$ and Rossby number $v_u(w/2)/w$, both based on values at the right channel wall ($x=w/2$). The value of the latter for all plots shown is 0.2. (Nof 1986, Figure 7.)

Figure 3.5.7 The change in potential vorticity across the shocks shown in Figure 3.5.6. (Nof, 1986, Figure 10.)

Figure 3.5.8 Schematic of a nonrotating hydraulic jump produced in a channel with a parabolic bottom. (Figure 7 of Siddall, et al. 2004).

Figure 3.5.9 Plan view of the jump suggested in Figure 3.5.8, as produced in a numerical simulation. The sudden change in depth occurs within the dashed area. The arrows indicate the depth-integrated velocity. (Figure 8 of Siddall, 2004).

Figure 3.5.10 Satellite photo showing sea surface glint around the Windward Islands. (NASA image S1998199160118, free of licensing fees but NASA ownership must be acknowledged)

Figure 3.5.11 Idealized plan view of hydraulic jump and wake in the lee of an obstacle. The large arrows indicate vorticity fluxes. (Schär and Smith, 1993, Figure 2).

Figure 3.5.12 Landsat 7 image of a vortex street as apparent in the cloud cover off the Chilean coast near the Juan Fernandez Islands on September 15, 1999. (NASA image Vortex-street-1.jpg.)

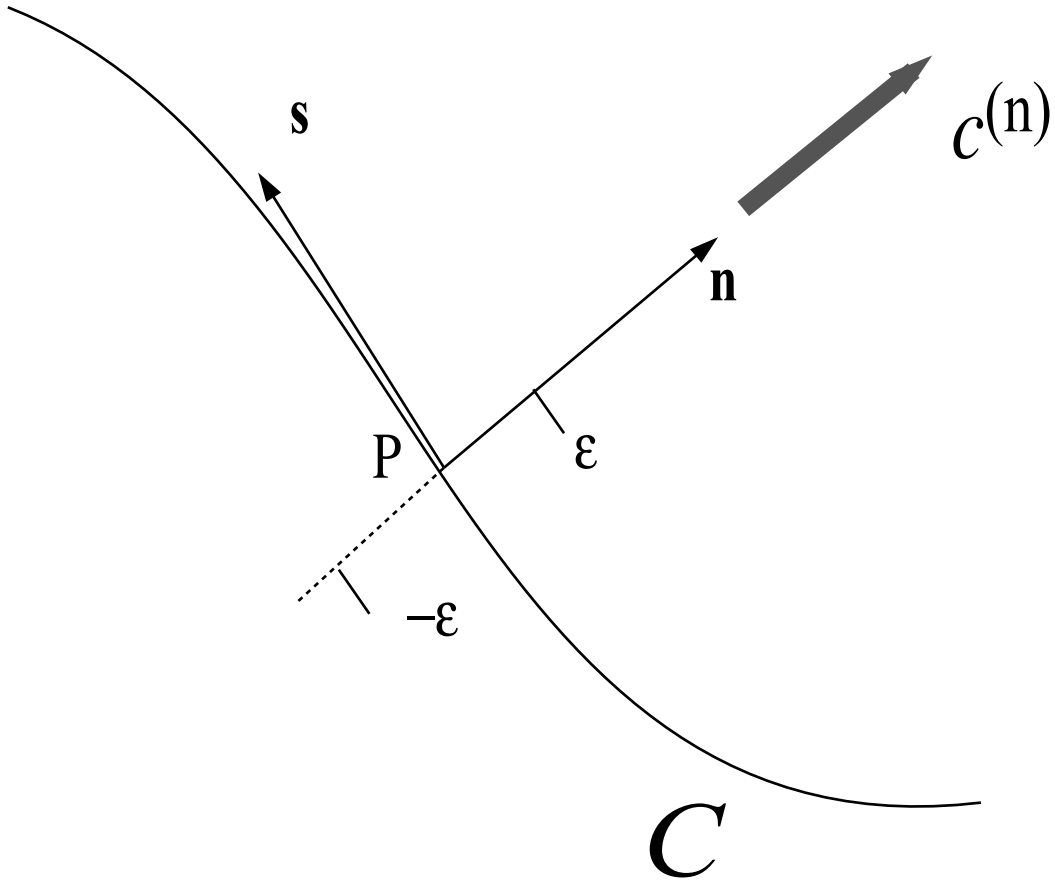

Figure 3.5.1

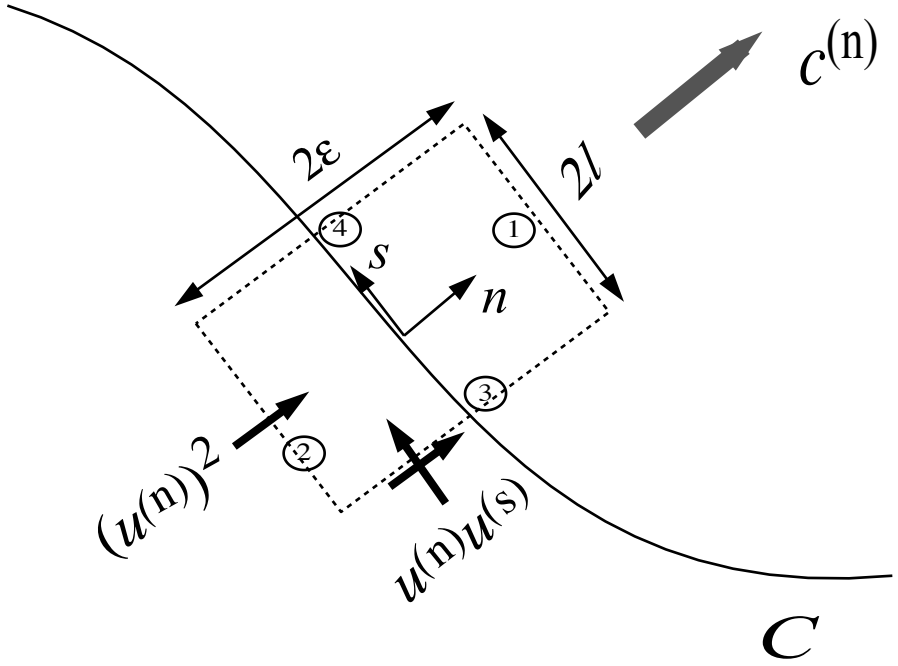

(a)

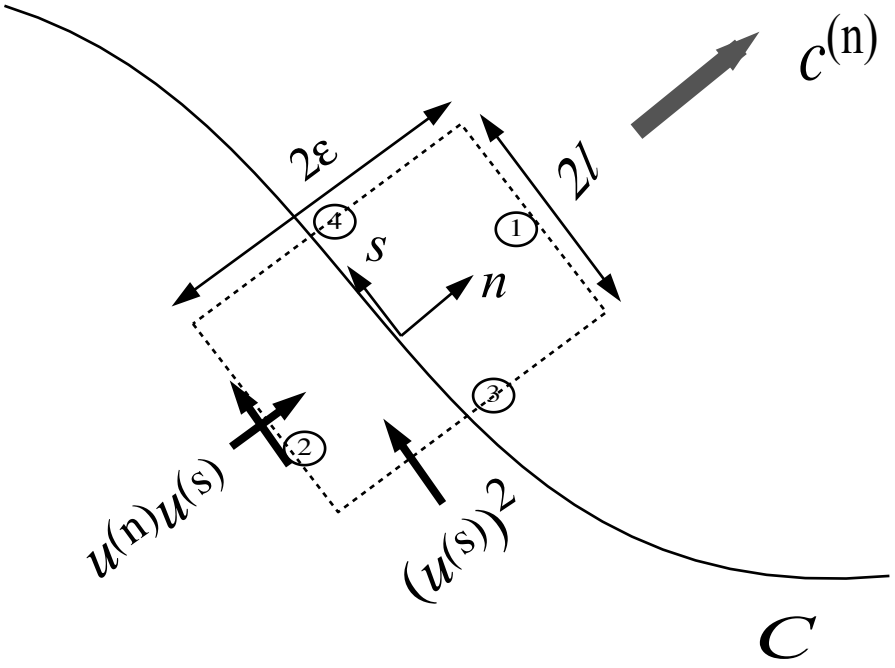

(b)

Figure 3.5.2

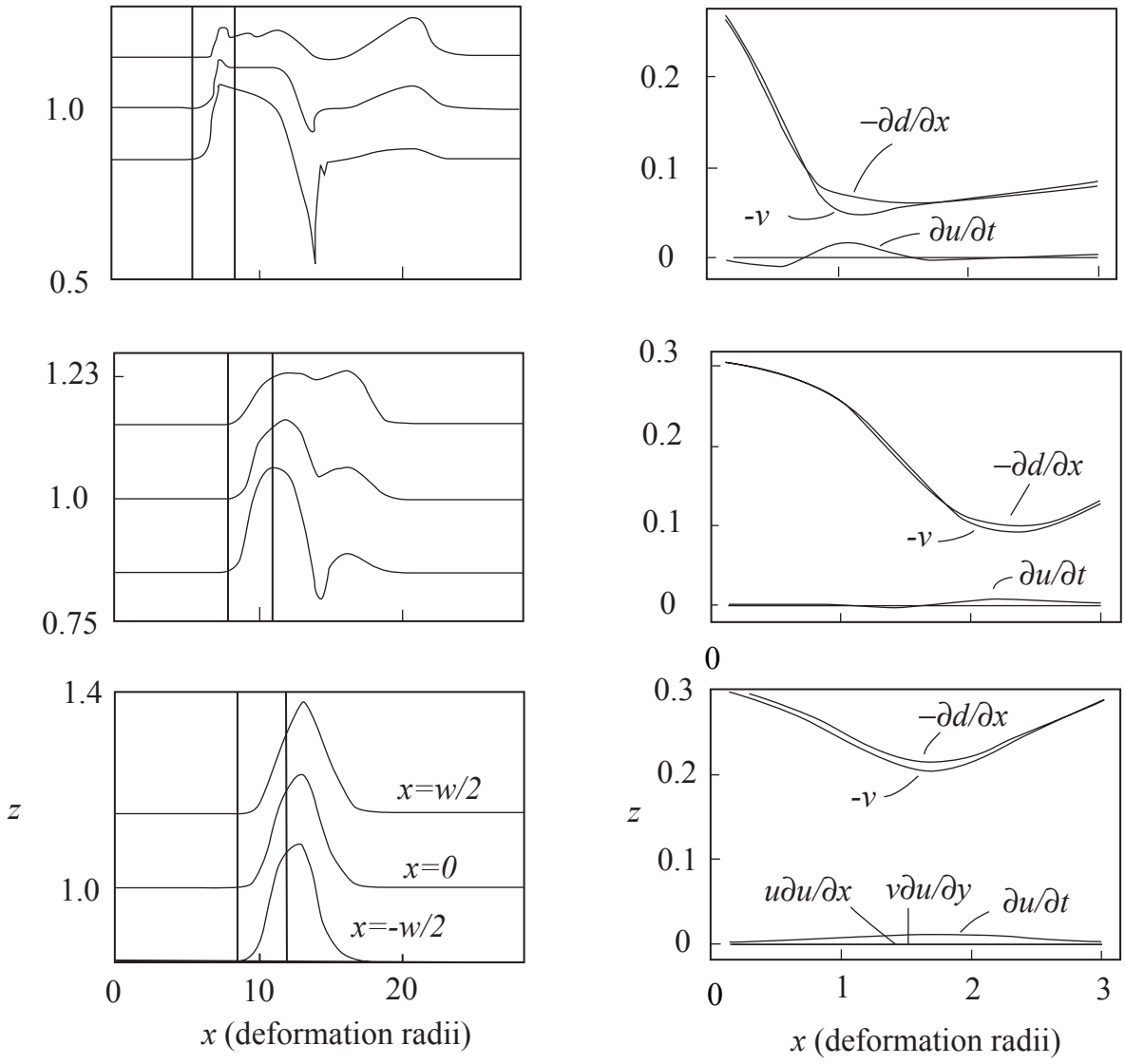

Figure 3.5.3.cs2.ai

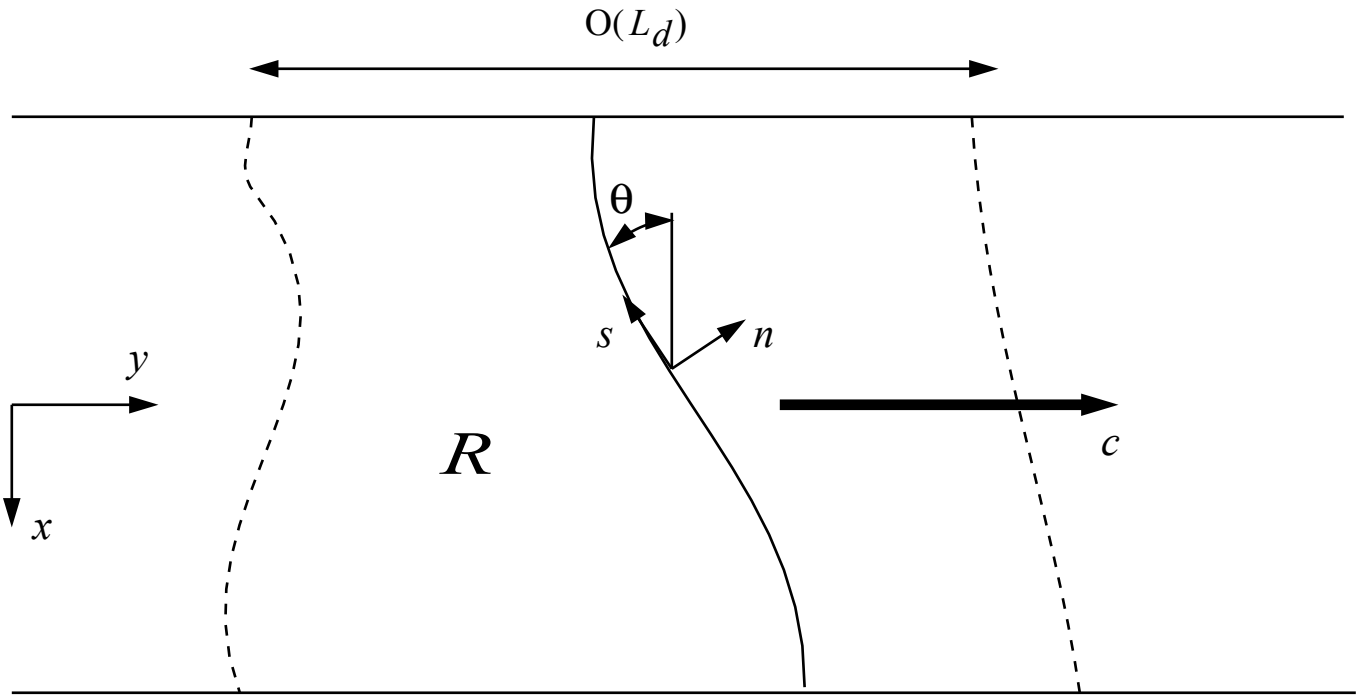

Figure 3.5.4

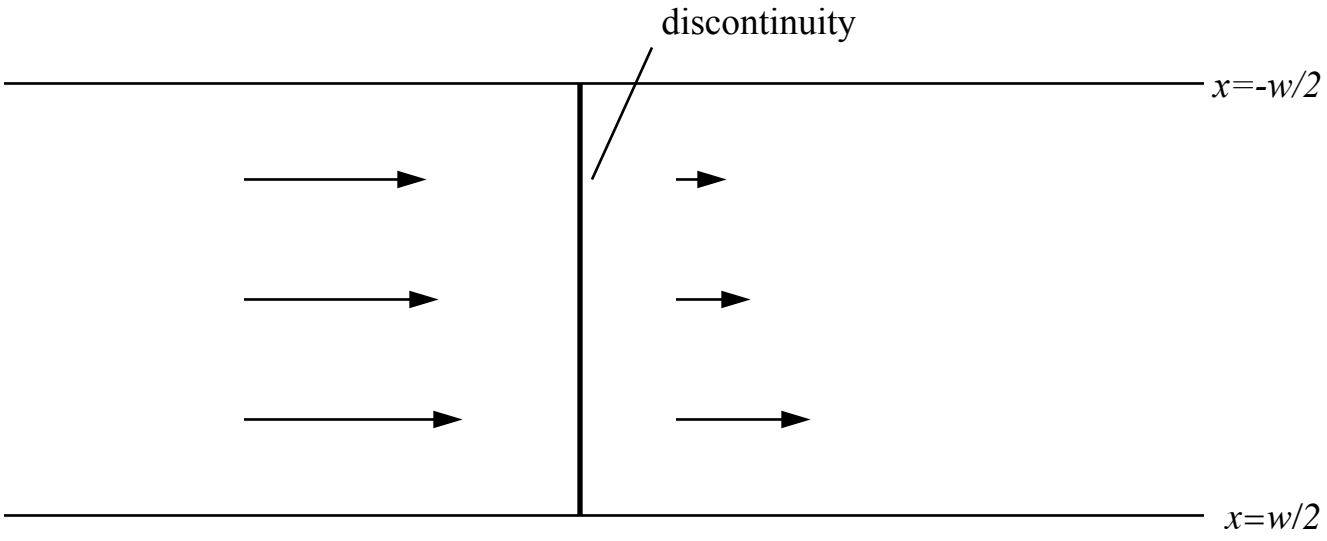

Figure 3.5.5

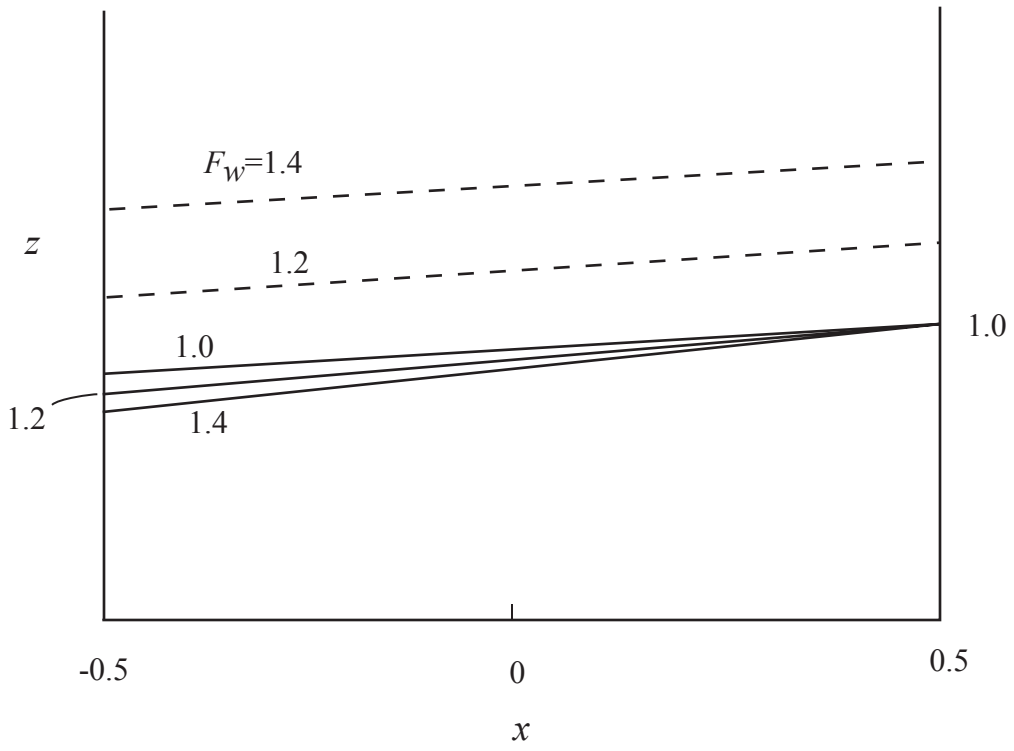

Figure 3.5.6

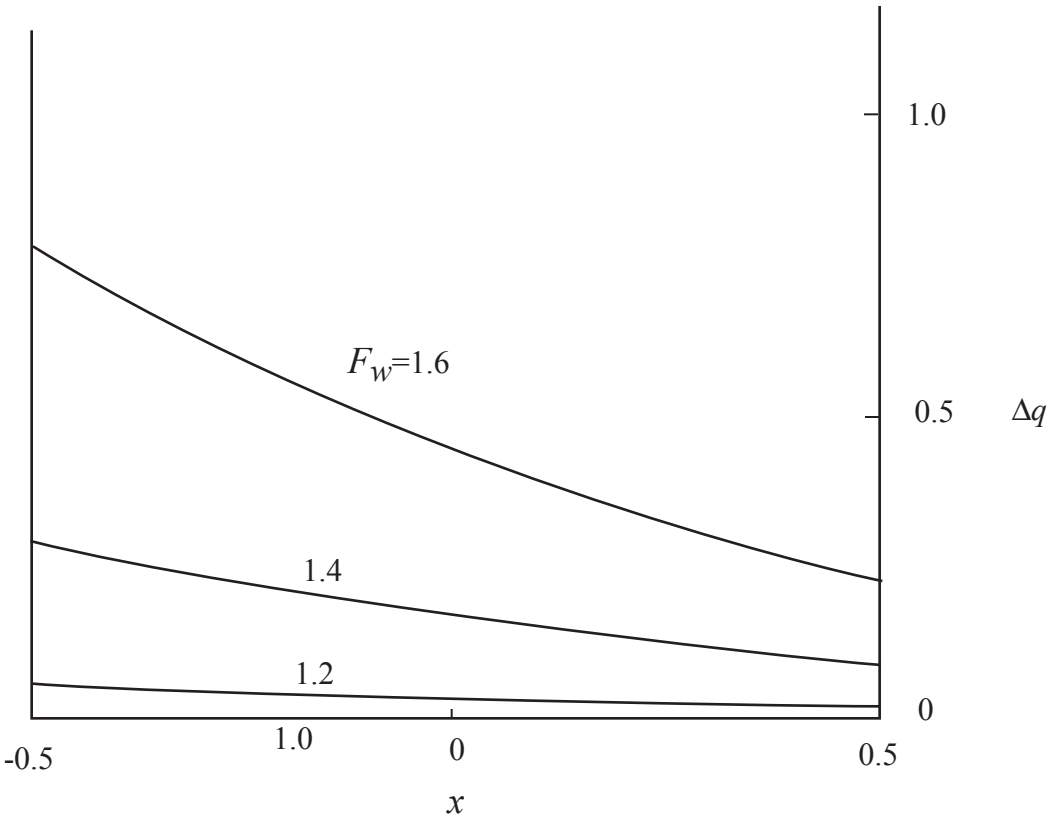

Figure 3.5.7

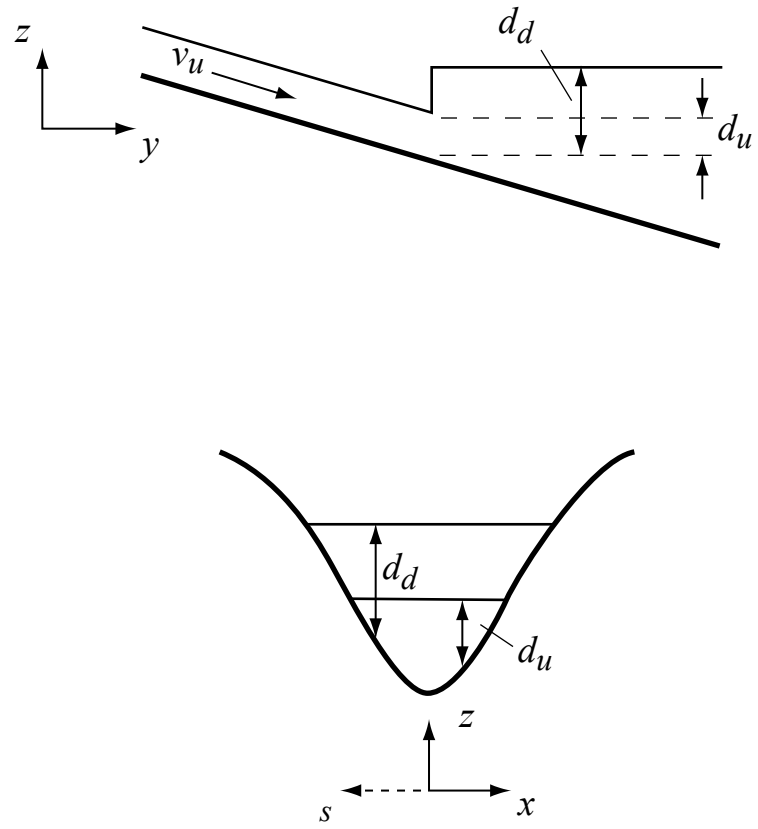

Figure 3.5.8

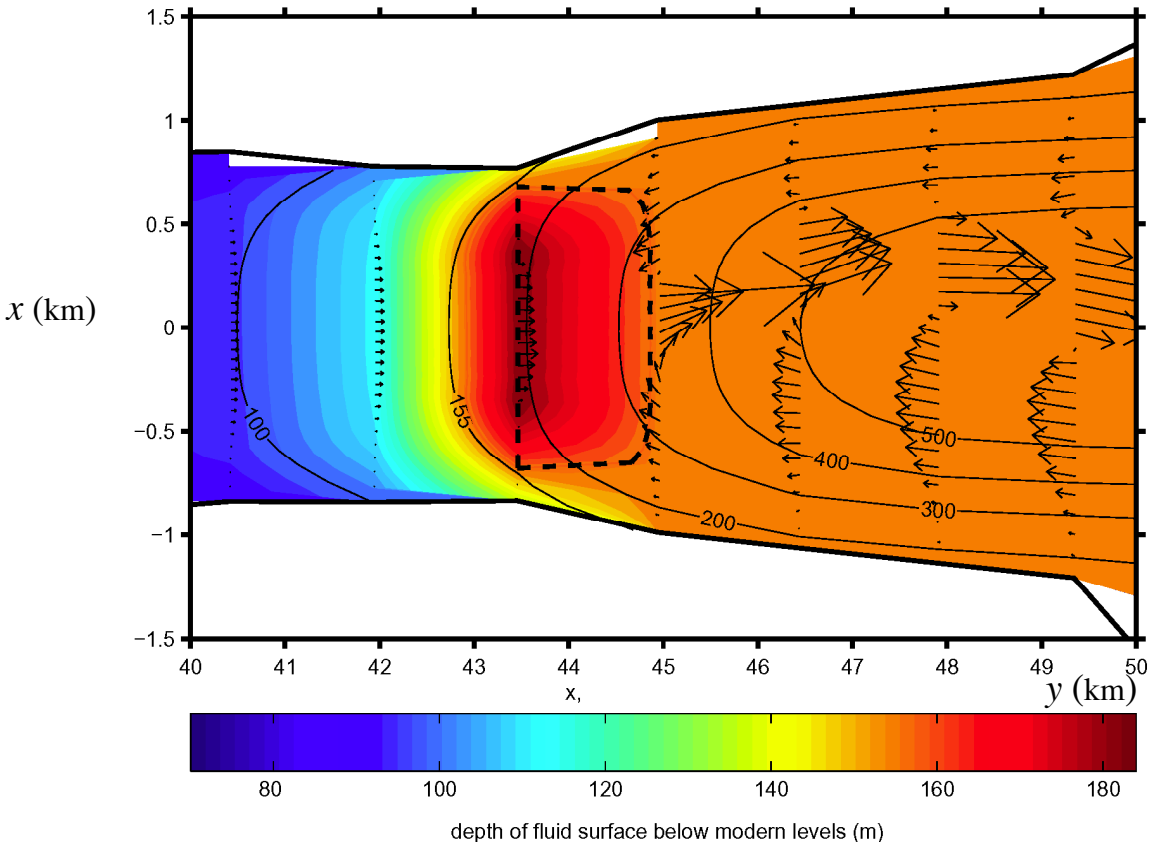
x (km)
1.5
1
0.5
0
−0.5
−1
−1.5
100
155
200
300
400
500
40
41
42
43
44
45
46
47
48
49
50
x,
y (km)
80
100
120
140
160
180
depth of fluid surface below modern levels (m)

Figure 3.5.9

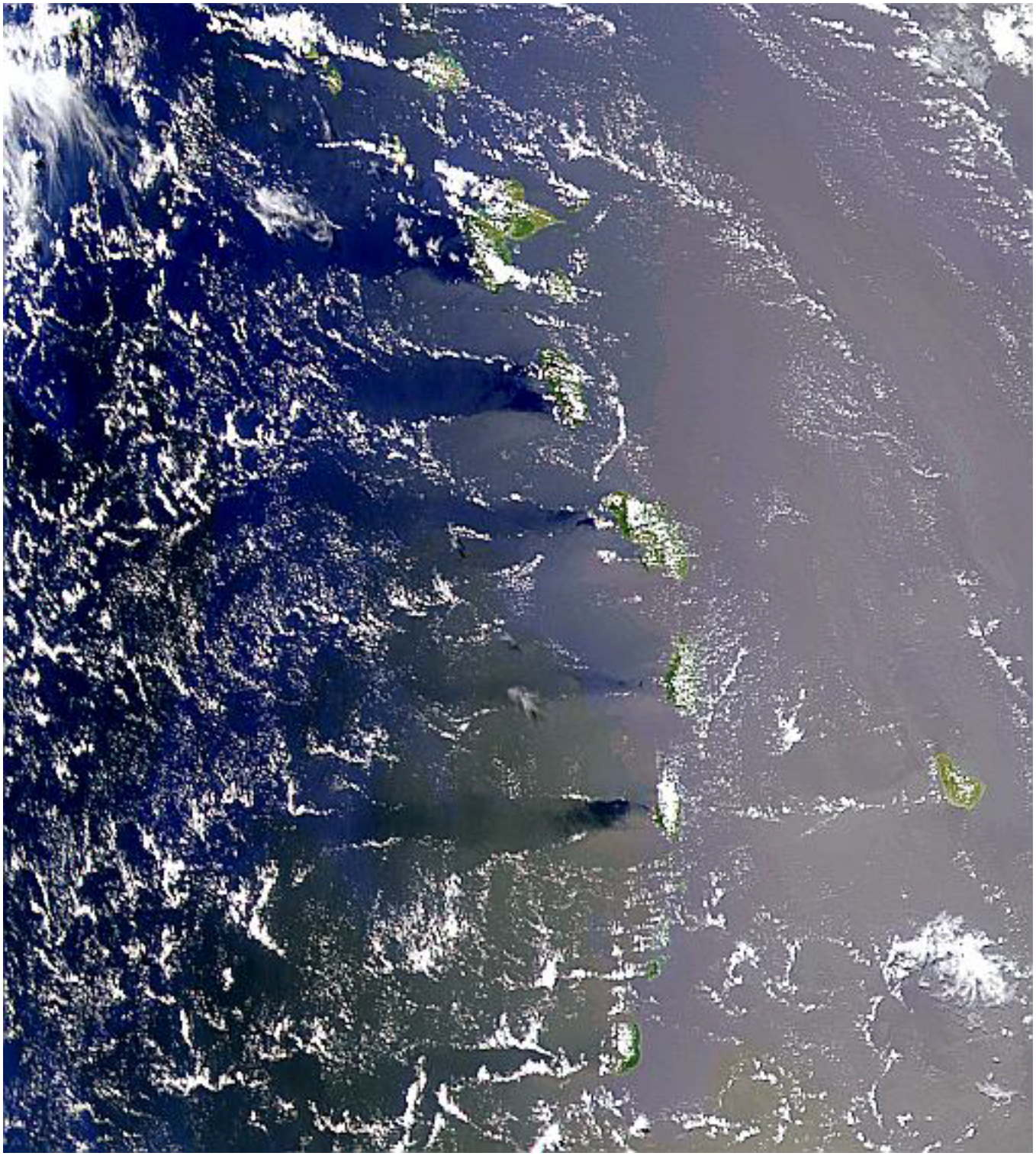

Figure 3.5.10

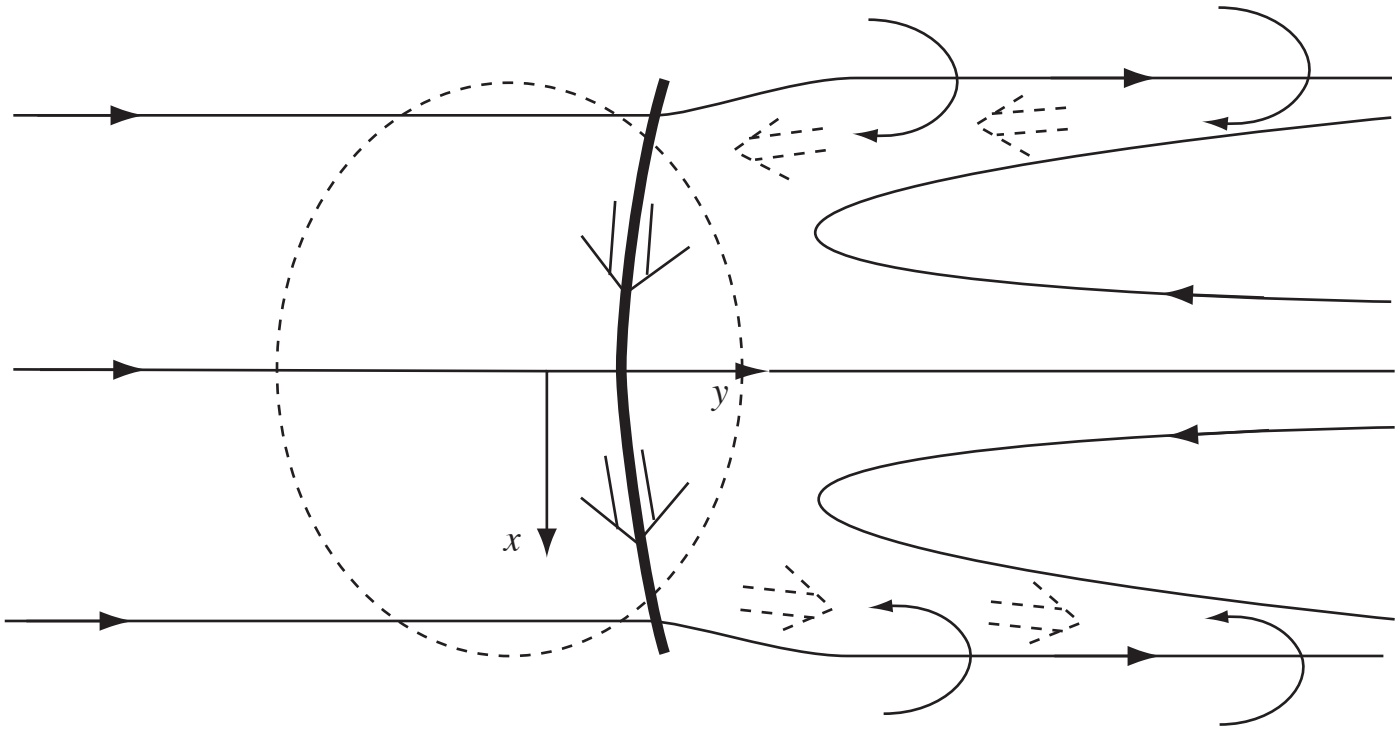

Figure 3.5.11

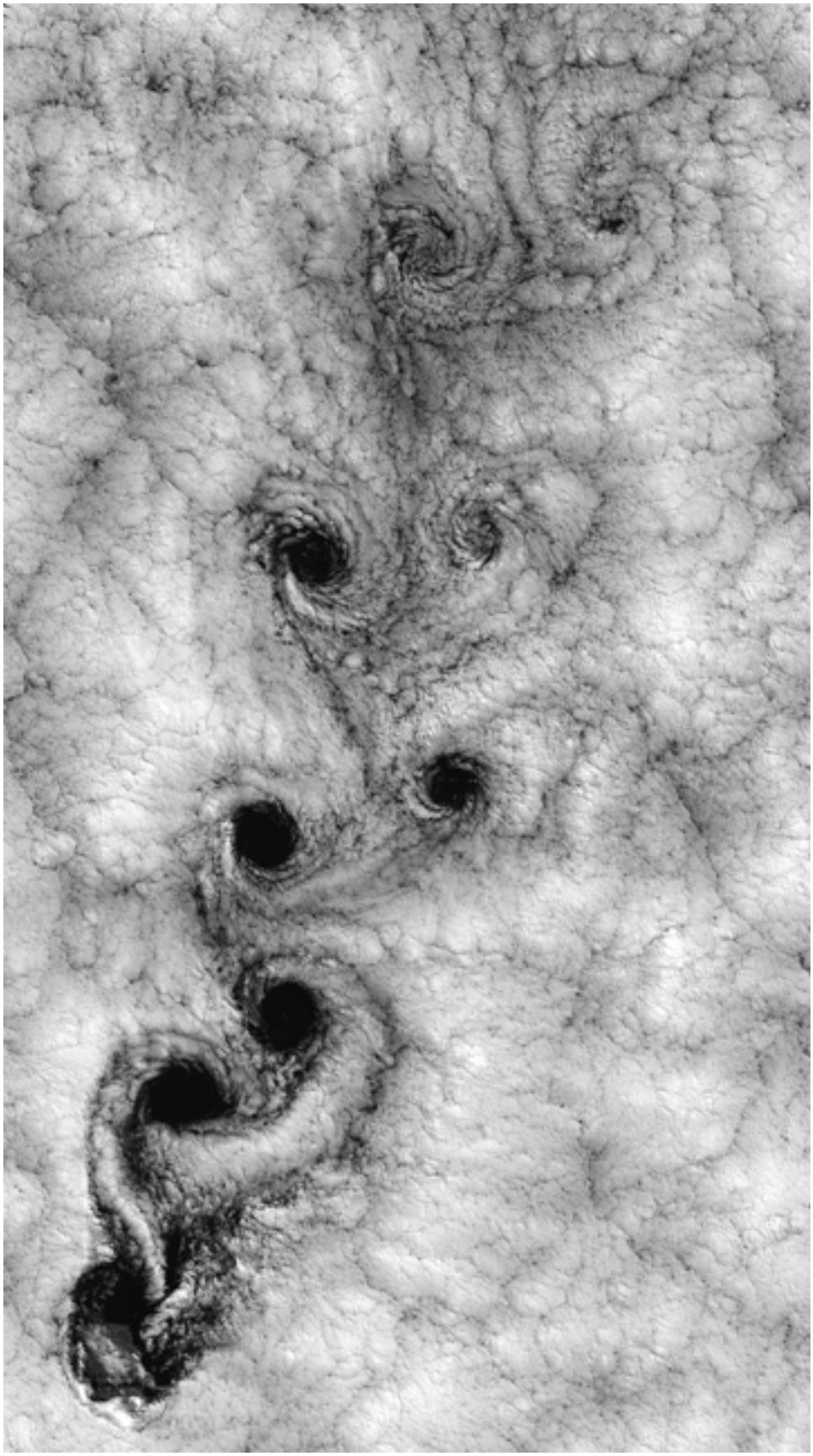

Figure 3.5.12 (low resolution version)